Tribological changes of tooth enamel-mullite/3Y-TZP couple in artificial saliva

Yanqi Huang

Central South University

Zhuan Li (✉ lizhuan@csu.edu.cn)

Central South University   https://orcid.org/0000-0003-3093-1941

Peng-fei Liu

Aalborg Universitet

Yan-meng Cheng

Central South University

Wen-jie Li

Central South University

Peng Xiao

Central South University

Abstract

In-situ mullite toughened 3Y-TZP composite ceramic (mullite/3Y-TZP) with excellent mechanical properties was fabricated by gel-casting. The cytotoxicity of mullite/3Y-TZP was determined by both extract and direct contact methods, and the results indicated that mullite/3Y-TZP had no acute cytotoxicity. Furthermore, the tribological properties of the tooth enamel sliding against mullite/3Y-TZP in artificial saliva were investigated by using the pin-on-plate friction method. The friction coefficient (μ) between the two friction samples was about 0.464 with a stable friction process, and both of them showed slight wear. Analysis of the wear surface and debris demonstrated that the tooth enamel mainly suffered from fatigue wear accompanied by mild adhesive wear, while mullite/3Y-TZP showed slight abrasive wear. This result indicated that mullite/3Y-TZP had good wear resistance and showed potential applications in dental material.

Highlights

1. In-situ mullite toughened 3Y-TZP composite ceramics has been prepared by gel-casting, and the biotoxicity of mullite/3Y-TZP composites has been systematic studied, providing a precondition for its biomedical applications.
2. It reveals the bio-tribological behaviour and wear mechanism of mullite/3Y-TZP composites sliding against tooth enamel in artificial saliva environment, providing a theoretical basis for its practical dental applications.

1. Introduction

Advanced biomaterials made of metals and ceramics have received extensive attention and developed rapidly over the last few decades with the improvement of medical level and the development of materials [1-5]. It is well known that biomaterials, especially dental materials, must have the characteristics of good biocompatibility, chemical stability and mechanical properties [6, 7]. Metal alloys, such as titanium alloys, are generally considered to be bio-inert in human biological systems. However, when they are used in the oral environment, the frequent interaction between alloys and physiological environment will release metal ions, which not only limits their long-term stability in vivo, but also is harmful to the patients' health [8-11].

Zirconia (ZrO_2) ceramic, as one of the most important oxide ceramics, not only in possession of bio-safety (no cytotoxicity), but also can exist stably in the oral environment without releasing harmful impurities and degradation [12-16]. In comparison with alumina (Al_2O_3) ceramic, ZrO_2 ceramic has more excellent mechanical properties, which can meet the requirements of higher compressive strength and hardness of dental crown [17-21]. Moreover, previous studies have confirmed that ZrO_2 ceramic shows poor bacterial adhesion. Scarano et al [22]. found that the coverage degree of bacteria on ZrO_2 was 12.1% as compared to 19.3% on titanium. Rimondini et al [22]. also confirmed these results through in-vivo studies, and their results indicated that Y-TZP accumulated fewer bacteria than that of titanium in

the total number of bacteria. Quinn et al [23]. studied the effects of microstructure and chemical composition on the mechanical properties of dental ceramics, and also believed that ZrO_2 ceramic had better mechanical properties than that of dental ceramics.

Despite ZrO_2 ceramic has high hardness, strength as well as good biocompatibility, the inherent brittleness limits its application. Mullite/3Y-TZP, as one of the ZrO_2 composite ceramics, not only improves the flexural strength and fracture toughness of pure ZrO_2 ceramic without introducing toxic composition, but also retains high hardness, which has been confirmed in our previous research [24, 25]. Nevertheless, in order to determine whether it is a better candidate for dental materials than pure ZrO_2 ceramic, especially for dental crowns, further research is needed on the biotoxicity and tribological properties of mullite/3Y-TZP, which will play an important role in the service life and failure behavior of this material when used as a kind of dental ceramic.

Gergo Mitov et al [26]. used natural enamel to slide against Y-TZP ceramic treated in four different methods, and found that there was no significant linear correlation between the ceramic surface roughness and abrasive wear. Wang et al [27]. studied the wear behavior of tooth enamel sliding against three kinds of dental ceramics (smooth and rough zirconia ceramics, glass ceramic, silicate-based veneer porcelain) with gold-palladium alloy and nickel-chromium alloy as control groups, and the results showed that the frictional coefficient of enamel sliding against polished zirconia or porcelain was between that of metal and glass-ceramic. Enamel showed abrasive wear when sliding against rough zirconia or glass ceramic, while fatigue wear was found on the worn surfaces of enamel when sliding against polished zirconia or nickel-chromium alloy, which showed that the friction and wear performance of zirconia can be improved significantly by proper surface polishing. Therefore, as a dental material, studying the oral tribological behavior of mullite/3Y-TZP is very important.

In the previous study, high-performance mullite/3Y-TZP has been prepared by gel-casting combined with pressureless sintering. Based on the comprehensive analysis of mechanical properties and microstructure of this ceramic, its biological toxicity will be confirmed by in vitro cytotoxicity tests including extract and direct contact methods in this study. These methods can be standardized to yield the repeatable results as well as efficiently performed at a relatively low cost [28, 29]. Moreover, the tribological properties of mullite/3Y-TZP will be deeply analyzed in terms of biology, including the study of wear behavior of the tooth enamel sliding against mullite/3Y-TZP in artificial saliva environment, and revealing their wear mechanism and wear resistance.

2. Experimental Procedures

2.1 Sample preparation

In this study, four human molars without obvious wear scar were derived from 18-year-old females, and were stored in physiological saline for sample preparation after being removed from the body. In order to prevent the original scratches on the enamel surface from affecting the observation of the morphology

after the tribological tests and test the roughness of the enamel surface more accurately, each tooth was polished on carborundum sandpaper from 400 to 2000 mesh in water, and then polished by polishing cloth. This treatment method was performed within the range of not affecting the structure and performance of enamel. Finally, those teeth were cold-set by resin to obtain columnar pins with the size of φ10mm×15mm, and the enamel surface was exposed.

Commercially available ZrO_2 powders (AR grade, Shanghai Chemical Regent Co., China), SiO_2 powders (AR grade, Shanghai Chemical Regent Co., China) and Al_2O_3 powders (Sinopharm Chemical Reagent Co., Ltd., China) were used as raw materials. Y_2O_3 powders (Changsha Deli Rare Earth Chemical Co., Ltd. China) were used as sintering aids. Using gel-casting method (AM-MBAM system) combined with pressureless sintering to prepare cuboid mullite/3Y-TZP with the dimensions of 25mm×25mm×15mm. More details about this experimental process and raw materials used in this study were described in the Ref. 26. The polishing steps of these samples were similar to those for the teeth.

2.2 Characterization methods

The optical density (OD) of the medium in porous plate was measured by absorbance microplate reader (ELx 800, USA). The morphologies of cells cultured with extract and direct contact methods were observed by inverted microscopy. Scanning electron microscope (SEM, JSM-6390, JEOL, Tokyo, Japan) was used to observe the surface morphologies of mullite/3Y-TZP and tooth enamel before and after tribological tests as well as wear debris. Using raman spectrum to analyze elemental composition and chemical bond information of mullite/3Y-TZP before and after tribological tests. X-ray diffraction (XRD, Cu Ka radiation, D/max-2550−18kW, Rigaku, Japan) from 15° to 70° at 40kV with a scanning speed of 8°/min, coupled with energy dispersive X-ray spectroscopy (EDS) were used to analyze elemental composition and phase of mullite/3Y-TZP before and after experiments as well as wear debris. The elemental distribution of the wear surface of mullite/3Y-TZP after experiments was analyzed by electron probe microanalysis (EPMA). Using atomic force microscopy (AFM) and laser scanning confocal microscope (LSM700, Zeiss, Germany) to measure surface roughness (Ra) of the polished tooth enamel and mullite/3Y-TZP as well as undulating state of the wear surface. Ultra depth of field three-dimensional microscopy system (VHX-500, Keyence, Japan) combine with LSM700 were used to characterize 3D morphologies of wear surface to determine width and depth of the wear track.

2.3 Cytotoxicity tests

In vitro cytotoxicity assays were carried out on mullite/3Y-TZP according to ISO10993-5 using both extract and direct contact methods [30, 31]. The extract assays used L929 mouse fibroblasts as test cells. Each sample was ground into a cube of 6×6×6mm, and then they were ultrasonically cleaned with alcohol and deionized water, and finally put them into autoclave for disinfection (121℃, 30min). Pure 3Y-ZrO_2 ceramic and mullite ceramic were used as experimental control groups, while the negative and positive control groups were also set. The flow diagram of the extract method is shown in **Fig. 1**, and the specific steps are as follows:

(1) Three different groups of the samples were placed in the complete medium for 24h after disinfection, and the ratio of the sample surface area to the volume of the culture medium was 1 and $3cm^2/mL$;

(2) After the cells resuscitated and adhered to the wall for growth, the original culture medium was removed and the sample extract was added. 6 holes were set for each concentration of each sample group, and then put them in the CO_2 incubator for 1, 3 and 5 days, respectively;

(3) The viability of cells was assessed by tetrazolium salt (MTT), and ELx 800 was used to detect the OD value of each hole [32]. Then, calculating relative growth rate (RGR) value according to the optical density (OD) value, and determining the cytotoxicity of the samples by combining with the cell morphologies.

Direct contact assays were performed using L929 mouse fibroblast. A cell suspension with the concentration of 5×10^4 cells/ml was dropped into a petri dish containing the sample, and the ratio of the sample surface area to the volume of the culture medium was 1:1. After being cultured in CO_2 incubator for 1, 3 and 5 days, using inverted microscopy to observe the cell morphologies and determine whether there were transparent areas around the samples.

2.4 Tribological tests

All tribological tests were carried out using pin-on-plate reciprocating friction method on the UMT-3 multifunctional friction and wear tester in artificial saliva conditions. The **device** and schematic diagram of the tribological tests are shown in **Fig. 2**. The tests used teeth as bolts, while polished mullite/3Y-TZP were used as counterparts. During the chewing process of human beings, the chewing force between the upper and lower teeth in the mouth ranges from 3 to 36N and the sliding distance between the bite contacted teeth is about 0.9-1.2 mm.[33-35]. Therefore, A normal force of 20 N, cyclic reciprocating displacement of 1mm, and frequency of 2 Hz were used in all tribological tests, as shown in Table 1. During the tests, the wear surfaces of these two friction components were always immersed in artificial saliva, and the contents of various components of artificial saliva are shown in Table 2 [27, 36]. The experiment was repeated three times in each condition. After tribological tests, the teeth and counterparts were ultrasonically cleaned and dried, and the wear rate was replaced by mass loss. (The mass loss of this friction couple was very low after tribological tests, and it was found that their wear rate was less than 1/10000 after rough calculation. In addition, non-regular structure of the tooth enamel selected in the experiment made it difficult to accurately express the wear rate by height loss. Therefore, it was more intuitive to demonstrate wear results by the mass loss.)

3. Results And Discussion

3.1 Cytotoxicity

The results of extract assays are shown in **Fig. 3** and **Fig. 4**. The data have been analysed by one-way ANOVA, and the minimum significant difference at $p < 0.05$ has been calculated and displayed on the histograms. There were no significant differences between any extracts of sample groups and the

negative control group except the mullite group. A significant decrease of OD value happened in the positive control group, indicating that the tests were valid and L929 mouse fibroblasts cells were susceptible to the degrees of cytotoxicity.

The OD values (490nm) of each set of samples are shown in **Fig. 3**. Low OD values of all experimental groups were found after the cells had been cultured by extracts for 1 day, which was mainly because the cells did not fully grow and divide, and the cell concentration was low. Three days later, the OD values increased significantly except for the pure mullite group with a concentration of $3cm^2$/mL and the positive control group. After being incubated for five days, the OD values of each experimental group were almost twice that of the cells cultured for 1 day, and each of them was not lower than that of the negative control group except the pure mullite group and positive control group.

Combined with the comparison between RGR value (>100%) and determination standard of cytotoxicity level, ZrO_2 ceramic and mullite/3Y-TZP had no cytotoxicity, and morphologies of the cells of these groups also confirmed this result, as shown in **Fig. 4(a-b)** [32]. Although RGR value of mullite group ▢100%, the result of morphologies of the cells cultured by extract of mullite for 5 days indicated that mullite had no cytotoxicity or slight cytotoxicity compared with that of the positive and negative control groups, as shown in **Fig. 4(c-e)**.

No adverse reaction was observed in petri dishes by inverted microscopy in the direct contact experiments, and morphologies of the cells are shown in **Fig. 5**. As depicted in **Fig. 5(a-c)**, no abnormalities or dead cells were found around the samples, and no cell-free transparent regions were observed. Density and morphologies of the cells of these sample groups were similar to those of the negative control group (**Fig. 5(d)**), while there were significant death cells in the positive control group (**Fig. 5(e)**). The results showed that those three kinds of samples were no-cytotoxicity, which was a further proof of the previous experimental results.

3.2 Microstructure characterization

Fig. 6 shows the microstructure of mullite/3Y-TZP, and there are two obviously different phases in the sample. The preliminary experimental results proved that the black phase was mullite generated by the reaction of Al_2O_3 and SiO_2 during the sintering process, while the gray area was ZrO_2 [24, 25]. In the ternary eutectic system of Y_2O_3-SiO_2-Al_2O_3 formed by Y_2O_3 with SiO_2 and Al_2O_3, local liquid phase appeared in the sample at high temperature, then the contact reaction and nucleation occurred between SiO_2 and Al_2O_3. After that, the core of mullite crystal grew into the columnar crystal through mutual diffusion, as shown in **Fig. 6(a)** [37-41]. The size of the columnar mullite was about 10μm, as shown in **Fig. 6(b)**, and there were ZrO_2 particles uniformly distributed in the interior of mullite, which can improve the strength of columnar mullite by the pinning effect. Meanwhile, columnar mullite will also significantly enhance and toughen the composite ceramic for this reason. In addition, previous studies have shown that Y_2O_3 can enter the crystal lattice of ZrO_2 to stabilize the tetragonal/cubic phase [25].

The surface morphologies of the tooth enamel before the tribological tests are shown in **Fig. 6(c-d)**. It retained complete character with no protrusions or microcracks on the surface, providing a reliable premise for subsequent friction experiments. EDS analysis indicated that the main components of the tooth enamel surface were calcium and phosphorus, and the atomic ratio of the two elements was about 1.6:1, confirming that tooth enamel was indeed made of hydroxyapatite ($Ca_{10}(PO_4)_6(OH)_2$), as shown in **Fig. 6(d)**, which provided a theoretical basis for subsequent analysis of wear debris.

3.3 Wear behavior

3.3.1 Coefficient of friction (µ) and mass loss

Ra and 3D topographies of the polished tooth enamel and mullite/3Y-TZP before the tribological tests are shown in **Fig. 7**. Their Ra values were 33.6nm and 148.22nm respectively, indicating that the surfaces of these two kinds of materials using for the experiments were smooth, which can significantly reduce the frictional resistance (F_x) and µ [42]. As is known to us, there should be an appropriate µ when the dental ceramics, especially ceramic crowns, sliding against natural teeth, so as not to cause excessive wear on one side or affect the chewing of food. The results were obtained by repeating the friction experiments for three times, and one of them was shown in **Fig. 8**. It can be seen that after a brief run-in period, the µ finally stabilized at 0.464. Combined with the results of Wang et al. (as shown in **Fig.9**), this value was between the µ of glass ceramics and Au-Pd alloy when rubbing against tooth enamel, and was particularly similar to the result of polished zirconia and porcelain [27]. Meanwhile, we also understood the influence of the surface treatment on the results of friction experiments of dental ceramics from their research, and this is why the frictional couple were polished before the tests. The reason for getting this result was that even though the surfaces of this couple were very smooth before the tribological tests, they would be destroyed after the initial contact under the action of applied load, resulting in unstable µ and F_x until new wear surfaces were generated. In the process of stable friction, the existence of artificial saliva played an important role in lubrication and cooling, but also could wash away the debris generated during the friction process and clean the wear surface. Therefore, the µ and F_x were decreased and extremely stable, and they were the factors that determined the mass loss of the teeth and mullite/3Y-TZP [34, 42]. This frictional behavior indicated that there was a good match between the tooth enamel and mullite/3Y-TZP.

The mass loss of the teeth and mullite/3Y-TZP was very small, even though the former value was slightly higher than that of the later, both of them lost a few milligrams, only were 0.5±0.1mg and 0.3±0.1mg, indicating that the wear resistance of the friction couple was well in this environment. Stable friction process and low mass loss proved that mullite/3Y-TZP had application potential in the field of oral cavity.

Moreover, Lee et al [43]. found that ZrO_2 would undergo phase transition under the action of load during the friction process, and the low mass loss of mullite/3Y-TZP may partly attributed to transformation toughening induced by flash-temperature. In this study, the diffraction peaks of different ZrO_2 phases of

mullite/3Y-TZP did not show significant changes before and after the tribological tests, as shown in the XRD patterns of **Fig. 10**. The diffraction peaks intensity of m-ZrO_2, t-ZrO_2 and c-ZrO_2 were almost unchanged, which may be caused by stress dispersion and cooling effects of artificial saliva. In addition, the internal structure of mullite/3Y-TZP did not change before and after the tribological tests, as shown in the Raman spectrum of **Fig. 11** (black and red curves). The intensity of the diffraction peak and Raman shift of m-ZrO_2 and t-ZrO_2 did not change significantly [44]. The -OH peak (3625cm^{-1}) was observed in the Raman spectrum of mullite/3Y-TZP after the tribological tests, and Lang et al. [45, 46] mentioned that Y_2O_3 could react with water to form α-$Y(OH)_3$ due to the action of water and pressure during the friction process. However, compared with the polished sample whose -OH peak most likely generated during the pretreatment process before the tribological tests, no new -OH peak formed during the friction process. This hypothesis was demonstrated by immersing mullite/3Y-TZP in artificial saliva for 5 days and then performing a Raman test, and the spectrum was shown in the blue curve. No significant changes happened in the intensity and Raman shift of the -OH peak, which was similar to those of the previous two results. These results indicated that mullite/3Y-TZP had good stability during friction and artificial saliva environments.

3.3.2 Wear appearances

Different observation methods were selected based on the different characteristics of the wear surface. 3D morphologies of the wear surface of the tooth enamel were measured by LSM700, and they showed a flat wear surface with almost no grooves or undulations, which can be obtained from **Fig. 12(a)**. Surface roughness of the wear surface was measured to be only 4.166μm, even though it was not as smooth as that of the original surface of tooth enamel, and the curve at the bottom of **Fig. 12(a)** also illustrated no significant fluctuation. This phenomenon may be caused by the formation of smooth film on the wear surface due to the deformation of the debris falling from tooth enamel under action of artificial saliva and load during the friction process, which indicated that no significant abrasive wear had occurred on the surface of enamel, providing a basis for the following wear mechanism. Mullite/3Y-TZP, as a counterpart, did not produce severe wear on its wear surface compared to enamel, as shown in **Fig. 12(b)**. The 3D morphologies measured by VHX-500 demonstrated that the worn area of mullite/3Y-TZP was very shallow, and the vertical height difference between the centre of the pit and the unworn surface was only 8.37μm, as shown by the curve below **Fig. 12(b)**. This was mainly because both mullite/3Y-TZP and enamel have high hardness, it was difficult to destroy the surface structure of mullite/3Y-TZP and cause serious wear during the friction process with the lubricating of artificial saliva,.

Fig. 13(a) represents overall appearance of the wear surface of enamel at low magnification, and it showed a flat surface without significant scratches, which was consistent with its 3D morphologies. **Fig. 13(b)** shows the morphology obtained by local magnification of **Fig. 13(a)**. A small amount of abrasive debris adhered to the flat surface, the analysis of EDS showed that they were calcium-phosphorus compounds (hydroxyapatite) derived from the surface of enamel, and contain a small amount of elements of mullite/3Y-TZP and artificial saliva, as shown in the upper right corner of **Fig. 13(b)**. **Fig. 13(c)** shows a portion of the edge of the worn region, and it was apparent that delamination of the

layered debris had occurred in this region, and the size was about 25μm, while cracks presented around it, which was closely related to stress-induced fatigue fracture.

Fig. 13(d) represents overall appearance of the wear surface of mullite/3Y-TZP at a low magnification, and only a very small amount of scratches presented on the flat surface. A small amount of abrasive debris adhered to the surface of the counterpart, and EDS analysis showed that their compositions were the same as that of the debris on enamel surface, as shown in **Fig. 13(e)**. Unlike the wear surface of enamel, the surface of mullite/3Y-TZP did not exhibit large-scale peeling, even though some scratches and microcracks appeared, as shown in **Fig. 13(f)**, which was closely related to the mechanical properties of mullite/3Y-TZP. In addition, the pinning effect of mullite and good combination between the ZrO_2 particles reduced the likelihood of particle flaking.

Similar study of Wang et al [27]. (as shown in **Fig. 14**) can be compared with the study in the text. **Fig. 14(a-c)** represents the wear surface morphology of enamel after sliding against polished zirconia ceramic, and the enamel surface generated micro cracks and a layer of wear debris, which was almost the same as the results of this study, indicating that the tooth enamel had appeared fatigue wear; What was different from the results of this experiment was that the wear surface of zirconia ceramic had obvious particle shedding phenomenon (as shown in **Fig. 14(d)**), that is, abrasive wear had occurred on the surface of zirconia ceramic, which was closely related to the brittleness of zirconia ceramic. Because mullite/3Y-TZP used in this experiment had better fracture toughness, the nailing effect of mullite and alumina particles reduced the possibility of zirconia particles falling off [24]. Fewer particles such as hard zirconia would reduce the damage to the friction couple during the friction process. Therefore, mullite/3Y-TZP is more suitable as dental materials than pure zirconia ceramic.

In order to further analyze element distribution of the wear surface of mullite/3Y-TZP, EPMA analysis was performed, as shown in **Fig. 15**, where Al and Si elements were not indicated. As shown in **Fig. 15(a-d)**, internal components Zr and Y of mullite/3Y-TZP were detected, and it clearly proved that Y element distributed uniformly in ZrO_2, which played a role in stabilizing t-ZrO_2. In addition to the components of ceramic matrix, there were also Ca and P elements on the wear surface, as shown in **Fig. 15(e-f)**, indicating that there was wear debris from enamel presented on the wear surface, which can be found in the grooves in combination with **Fig. 15(a)**. The representative elements of artificial saliva, such as Na, Cl, etc. also existed on the wear surface, and their distribution was consistent with that of Ca and P elements besides a small amount of them evenly distribute in other areas, which was mainly because of the adsorption of wear debris to artificial saliva. It was apparent that the filling of grooves and cavities with wear debris and artificial saliva can significantly lubricate the wear surface and reduce friction resistance.

3.3.3 Wear mechanism

The shape of the wear debris provides a reliable clue to the wear mechanism of the specimen. **Fig. 16** shows morphologies of the wear debris obtained after tooth enamel sliding against mullite/3Y-TZP in artificial saliva, from which abrasive grains and layered wear debris with different sizes can be seen.

Abrasive grains showed small sizes with obvious aggregation and mutual adhesion, while the layered debris had two kinds of morphologies: (Ⅰ) large layered debris with a rough surface, as shown in **Fig. 16(a-b)**, and (Ⅱ) layered debris with a smooth surface, as shown in **Fig. 16(c-d)**. On the surface of the first kind of lamellar debris, there were aggregated fine particles and obvious microcracks, which was caused by the aggregation of abrasive debris under the combined action of artificial saliva and load during the friction process, or directly from the lamellar shedding on the surface of the enamel. The second kind of lamellar debris had clear outline with distinctly straight boundaries and microcracks, indicating that they were mainly caused by brittle fracture. The elements of these wear debris were shown in **Fig. 17(a-d)**, it can be seen that the mass ratio of three elements of calcium, phosphorus and oxygen in the wear debris was high, reaching 26%, 18% and 24% respectively, which was consistent with the composition of enamel, and they were distributed almost every debris combined with **Fig. 17(a)**. In addition, the surface of the wear debris was evenly distributed with a small amount of debris from the surface of the mullite/3Y-TZP and elements in the artificial saliva, as shown in **Fig. 17(e-i)**, which indicated that only slight wear occurred in mullite/3Y-TZP, thus it was difficult to find large pieces of ZrO_2 particles in the wear debris. The filling and lubrication of the wear surface by artificial saliva reduced the frictional resistance and mass loss, and result in the adhesion of elements, such as Na and K on the surface of the enamel and counterpart.

The morphologies of the wear debris combined with the character of the wear surface indicated that enamel mainly experienced fatigue wear. Because enamel on the surface of tooth is hard and brittle, repeated friction and load will cause stress concentration in the contact part, resulting in fatigue fracture [34]. In addition, the shape of the edge portion of the wear surface indicated that adhesive wear happened locally (**Fig.13(a)**), which was due to the abrasive was wetted and pressed to form film on the wear surface, and then the film was peeled off due to repeated friction for a long time. Thereby, an adhesive wear zone was formed.

However, whether it was from the mass loss and wear surface morphologies of mullite/3Y-TZP or the elemental analysis of the wear debris, mild wear of mullite/3Y-TZP could be obtained. The uniform distribution of Zr, Al and Si elements in the wear debris indicated that mullite/3Y-TZP did have a slight particle flaking phenomenon and only occur mild abrasive wear, which was also consistent with a few scratches on its wear surface. The lubrication and cooling effects of the wear debris and artificial saliva which filled in the pits of the wear surfacec of mullite/3Y-TZP maintained the entire friction process at an extremely low mass loss during the repeated tribological tests. Because the hardness of the enamel was lower than that of mullite/3Y-TZP and artificial saliva had lubrication and cooling effects, it was difficult to cause extensive fatigue wear on the composite ceramic. In addition, almost no phase transformation of ZrO_2 was obtained by the previous XRD analysis during the friction process, and Raman analysis found no significant reaction between Y_2O_3 with water, indicating that the internal structure of mullite/3Y-TZP was retained, which played an important role in retaining high mechanical properties. This phenomenon showed that mullite/3Y-TZP had good stability and wear resistance in the human oral environment.

4. Conclusion

The cytotoxicity of mullite/3Y-TZP has been preliminarily studied based on its dental application, and the tribological properties of the tooth enamel sliding against mullite/3Y-TZP in artificial saliva environment have been deeply analyzed with mullite/3Y-TZP as the counterpart. The main conclusions are as follows:

1. The cytotoxicity of mullite/3Y-TZP was tested by both extract and direct contact methods. The results indicated that mullite/3Y-TZP did not show acute cytotoxicity like ZrO_2 ceramic, even though the second phase of mullite was introduced.

2. In artificial saliva environment, the friction process between the tooth enamel and mullite/3Y-TZP was extremely stable with the μ of 0.464, which was in the range of μ when natural teeth chewing food. The mass loss of the two materials was low due to the lubrication and cooling effects of artificial saliva. These tribological properties showed that the friction pairs matched well.

3. No significant phase transitions happened to mullite/3Y-TZP during the tribological tests. The tooth enamel mainly suffered from fatigue wear accompanied by slight adhesive wear due to the filling of artificial saliva and wear debris. While mullite/3Y-TZP only showed slight abrasive wear in this condition. These results indicated that mullite/3Y-TZP had good stability and wear resistance.

Declarations

References

1. Nath S, Basu B. Materials for orthopedic applications. *Adv Biomater.* John Wiley and Sons, Inc. 2010.
2. Fu S Y, Zhu M, Zhu Y. Organosilicon polymer-derived ceramics: An overview. *J Adv Ceram* 2019, **8**: 457-478.
3. Matasa C G. Trends in orthodontic biomaterials: metals and ceramics. *Orthod Fr* 2000, **71**: 335.
4. Affatato S, Ruggiero A, Merola M. Advanced biomaterials in hip joint arthroplasty. A review on polymer and ceramics composites as alternative bearings. *Compos Part B Eng* 2015, **83**: 276-283.
5. Afzal, Adeel. Implantable ZrO_2 bioceramics for bone repair and replacement: A chronological review. *Mater Express* 2014, **4**: 1-12.
6. Anselme K. Osteoblast adhesion on biomaterials. *Biomater* 2000, **21**: 667-681.
7. Sivakumar R. On the relevance and requirements of biomaterials. *B Mater Sci* 1999, **22**: 647-655.
8. Bandyopadhyay A, Bose S, Roy M, et al. MgO-doped tantalum coating on Ti: Microstructural study and biocompatibility evaluation. *Acs Appl Mater Inter* 2012, **4**: 577-580.

9. Scarano A, Piattelli M, Caputi S, et al. Bacterial adhesion on commercially pure titanium and zirconium oxide disks: an in vivo human study. *J Periodonto* 2004, **75**: 292-296.

10. Khan M A, Williams R L, Williams D F. In-vitro corrosion and wear of titanium alloys in the biological environment. *Biomater* 1996, **17**: 2117.

11. Hodgson A W E, Mueller Y, Forster D, et al. Electrochemical characterisation of passive films on Ti alloys under simulated biological conditions. *Electrochim Acta* 2003, **47**: 1913-1923.

12. Piconi C, Maccauro G. Zirconia as a ceramic biomaterial. Biomater 1999, 20: 1.

13. Afzal A. Implantable zirconia bioceramics for bone repair and replacement: A chronological review. *Mater Express* 2014, **4**: 1-12(12).

14. Christel P, Meunier A, Heller M, et al. Mechanical properties and short-term in vivo evaluation of yttria-oxide-partially-stabilized zirconia. *J Biomed Mater Res* 1989, **2**: 45-61.

15. Josset Y, Oum'Hamed Z, Zarrinpour A, et al. In vitro reactions of human osteoblasts in culture with zirconia and alumina ceramics. *J Biomed Mater Res* 2015, **47**: 481-493.

16. Carlo F D, Prosper L, Ripari F, et al. Bone response to zirconia ceramic implants; an experimental study in rabbit. *Key Eng Mater* 2001, **192-195**: 403-408.

17. Teng X, Liu H, Huang C. Effect of Al_2O_3, particle size on the mechanical properties of alumina-based ceramics. *Mater Sci Eng A* 2007, **452**: 545-551.

18. Vasylkiv O, Sakka Y, Skorokhod V V. Low-temperature processing and mechanical properties of zirconia and zirconia-alumina nanoceramics. *J Am Ceram Soc* 2003, **86**: 6.

19. Zhang Y, Vaßen, Robert, Mack D E, et al. Mechanical properties of zirconia composite ceramics. *Ceram Int* 2013, **39**: 7595-7603.

20. Pilathadka S, Vahalová D, Vosáhlo T. The Zirconia: a new dental ceramic material. An overview. *Prague Med Rep* **108**: 5-12.

21. Vagkopoulou T, Koutayas SO, Koidis P, et al. Zirconia in dentistry: Part 1. Discovering the nature of an upcoming bioceramic. *Eur J Esthet Dent* 2009, **4**: 130-151.

22. Rimondini L, Cerroni L, Carrassi A, et al. Bacterial colonization of zirconia ceramic surfaces: An in vitro and in vivo study. *Int J Oral Maxillofac Implants* 2002, **17**: 793-798.

23. Quinn J B, Sundar V, Lloyd I K. Influence of microstructure and chemistry on the fracture toughness of dental ceramics. *Dent Mater* 2003, **19**: 603-611.

24. Huang Y Q, Li Z, Liu P F, et al. Effects of the content of in-situ grown mullite on the microstructure and mechanical properties of 3Y-TZP ceramics fabricated by gel-casting. *Ceram Int* 2018, **44**: 21882-21892.

25. Liu P F, Li Z, Xiao P, et al. Microstructure and mechanical properties of in-situ grown mullite toughened 3Y-TZP zirconia ceramic fabricated by gel-casting. *Ceram Int* 2018, **44**: 1394-1403.

26. Gergo M, Siegward D, Stephanie W. Wear behavior of dental Y-TZP ceramic against natural enamel after different finishing procedures. *Dent Mater* 2012, **28**: 909-918.

27. Wang L, Liu Y H, Si W J, et al. Friction and wear behaviors of dental ceramics against natural tooth enamel. *J Eur Ceram Soc* 2012, **32**: 2599-2606.

28. Eldeniz A U, Mustafa K, Orstavik D, et al. Cytotoxicity of new resin-, calcium hydroxide- and silicon-based root sealers on fibroblasts derived from human gingiva and L929 cell lines. *Int Endod J* 2010, **40**: 329-337.

29. Williams D F. On the mechanisms of biocompatibility. *Biomater* 2008, **29**: 2941-2953.

30. ISO 10993-5. Biological evaluation of medical devices-Part 5: tests for in vitro cytotoxicity. International Organization for Standardization.

31. Mossman T. Rapid colorimetric assay for cellular growth and survival: application to proliferation and cytotoxicity assays. *J Immunol Methods* 1983, **65**: 55-63.

32. Ciapetti G, Cenni E, Pratelli L, et al. In vitro evaluation of cell/biomaterial interaction by MTT assay. *Biomater* 1993, **14**: 359-364.

33. Zhou Z R, Yu H Y, Zheng J, et al. Effect of the Oral Environment on the Tribological Behavior of Human Teeth. *Dent Biotribol* 2013: 75-115.

34. Riro B. Frontal-plane lateral border movements and chewing cycle characteristics. *J Oral Rehabil* 2001, **28**: 930-936.

35. Embong A, Glyn-Jones J, Harrison A. The wear effects of selected composites on restorative materials and enamel. *Dent Mater* 1987, **3**: 236-240.

36. Holland R I. Galvanic currents between gold and amalgam. *Scand J Dent Res* 1980, **88**: 269-272.

37. Zhu W W, Jiang H F, Zhang H. Effect of TiO_2 and CaF_2 on the crystallization behavior of Y_2O_3-Al_2O_3-SiO_2 glass ceramics. *Ceram Int* 2018, **44**: 6653-6658.

38. Mecartney M L. Influence of an amorphous second phase on the properties of yttria-stabilized tetragonal zirconia polycrystals (Y-TZP). *J Am Ceram Soc* 1987, **70**: 54-58.

39. Qin H, Huang X. Microstructure and bending strength of 3Y-TZP/12Ce-TZP ceramics fabricated by liquid-phase sintering at low temperature. *J Am Ceram Soc* 2000, **83**: 2881-2883.

40. Jr T J M, Laughner J W. Microstructures of mullite sintered from seeded sol-gels. *J Am Ceram Soc* 1989, **72**: 508-509.

41. Huang T, Rahaman M N, Mah T I, et al. Effect of SiO_2 and Y_2O_3 additives on the anisotropic grain growth of dense mullite. *J Mater Res* 2000, **15**: 718-726.

42. Buciumeanu M, Queiroz J R C, Martinelli A E, et al. The effect of surface treatment on the friction and wear behavior of dental Y-TZP ceramic against human enamel. *Tribol Int* 2017, **116**: 192-198.

43. Lee S W, Hsu S M, Shen M C. Ceramic wear maps: Zirconia. *J Am Ceram Soc* 2010, **76**: 1937-1947.

44. Tang X L, Zheng X H. Raman Scattering and t-Phase Lattice Vibration of 3% (mole fraction) Y_2O_3-ZrO_2. *J Mater Sci Technol* 2004, **20**: 485-489.

45. Monosmith W B, Walrafen G E. Temperature dependence of the Raman OH-stretching overtone from liquid water. *J Chem Phys* 1984, **81**: 669.

46. Lange F F, Dunlop G L, Davis B I. Degradation During Aging of Transformation -Toughened ZrO_2-Y_2O_3 Materials at 250°C. *J Am Ceram Soc* 2010, **69**: 237-240.

Tables

Table 1. Experimental parameters and results of the friction test

	Experimental parameters				Experimental conditions	Experimental results	
Specimen :Counterpart	Speed r/min	Load 〔N〕	Time min	Displacement mm	Environment	Average μ	Mass loss mg
Tooth :Mullite/3Y-TZP	180	30	60	1	Artificial saliva	0.464	0.5±0.1
							0.3±0.1

Table 2. Composition of artificial saliva

NaCl	KCl	$CaCl_2 \cdot 2H_2O$	$NaH_2PO_4 \cdot 2H_2O$	$Na_2S \cdot 9H_2O$	Urea	Distilled water
0.4g	0.4g	0.795g	0.78g	0.005g	1g	1000mL

Figures
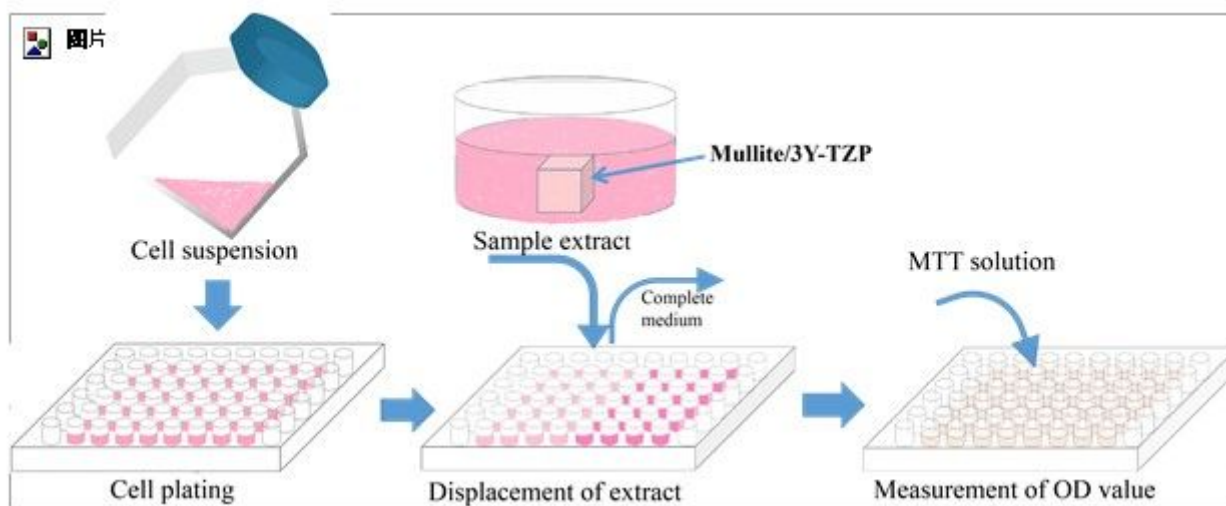
Figure 1

Flow diagram of the extract method.
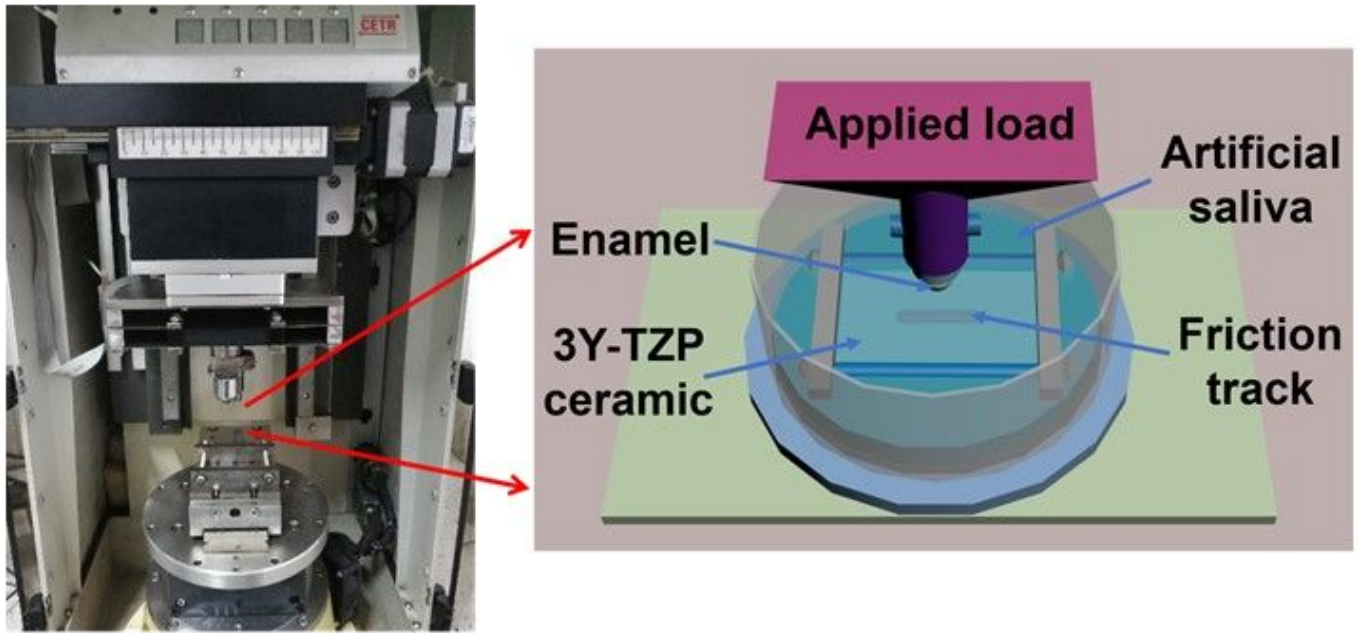
Figure 2

Device diagram and schematic diagram of the friction test.
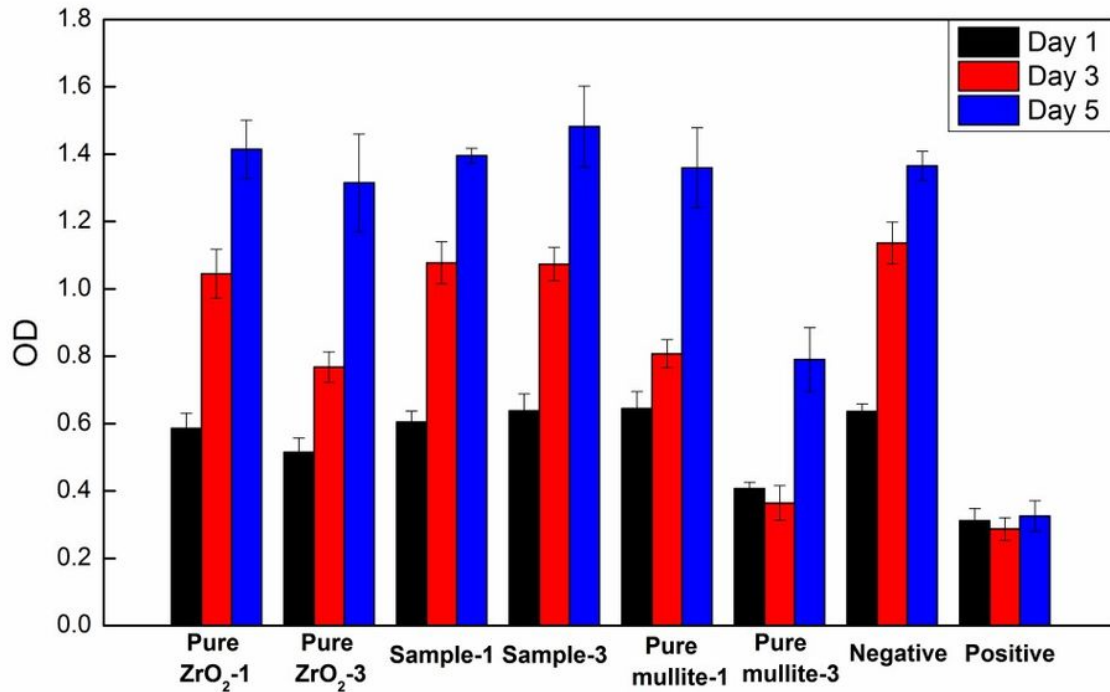
Figure 3

Cytotoxicity assessment of each group of sample using L929 mouse fibroblast.
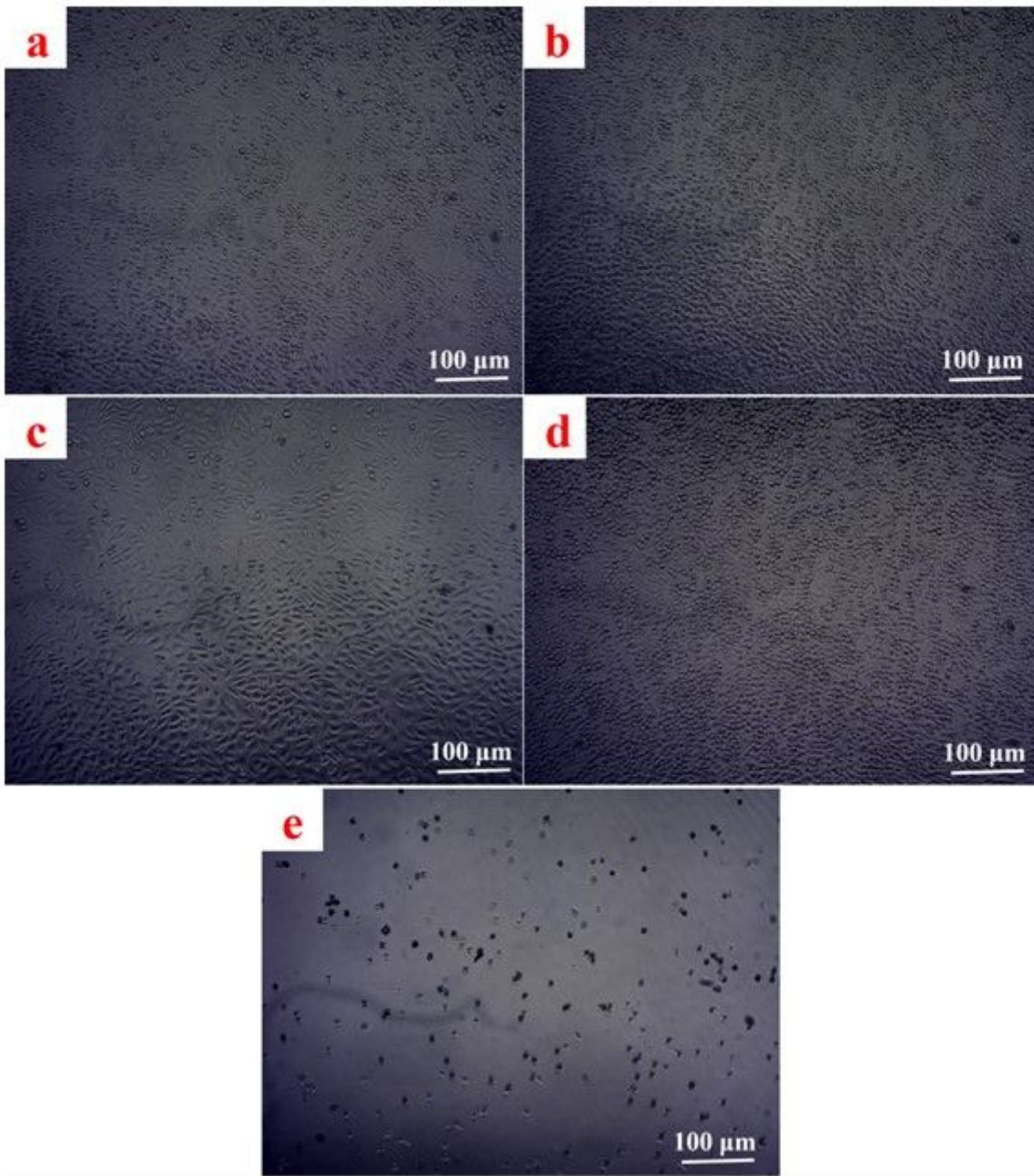
Figure 4

Morphologies of cells cultured at 3cm2/mL for 5 days in different groups. (a-c): extract of mullite/3Y-TZP, 3Y-TZP and mullite; (d-e): Negative and positive control groups.
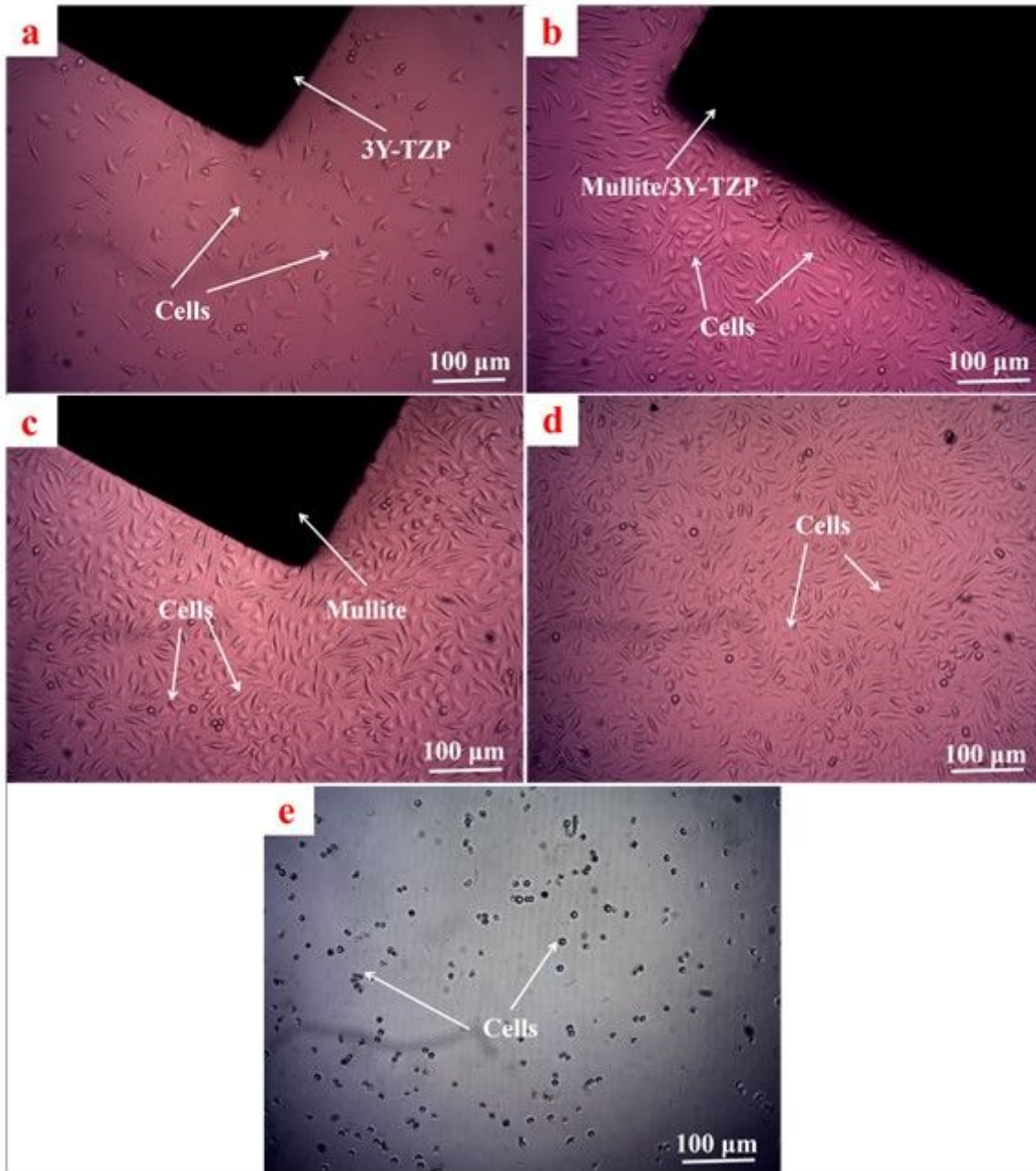
Figure 5

Morphologies of cells cultured for 5 days by the direct contact method. (a-c): The groups of mullite/3Y-TZP, 3Y-TZP and mullite; (d-e): Negative and positive control groups.
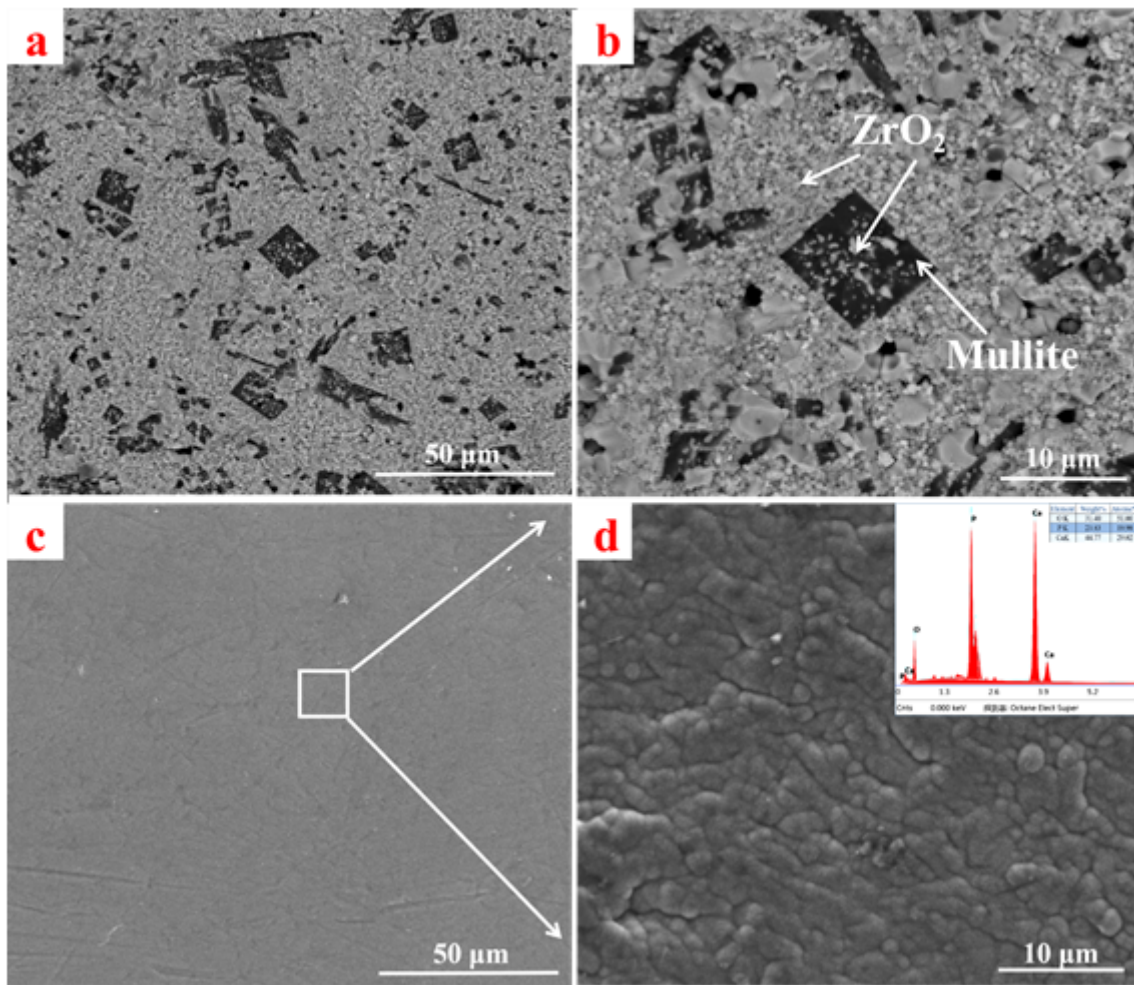
Figure 6

6.(a-b): SEM images of the surface of mullite/3Y-TZP; (c-d): SEM images and EDS of the surface of the tooth enamel.
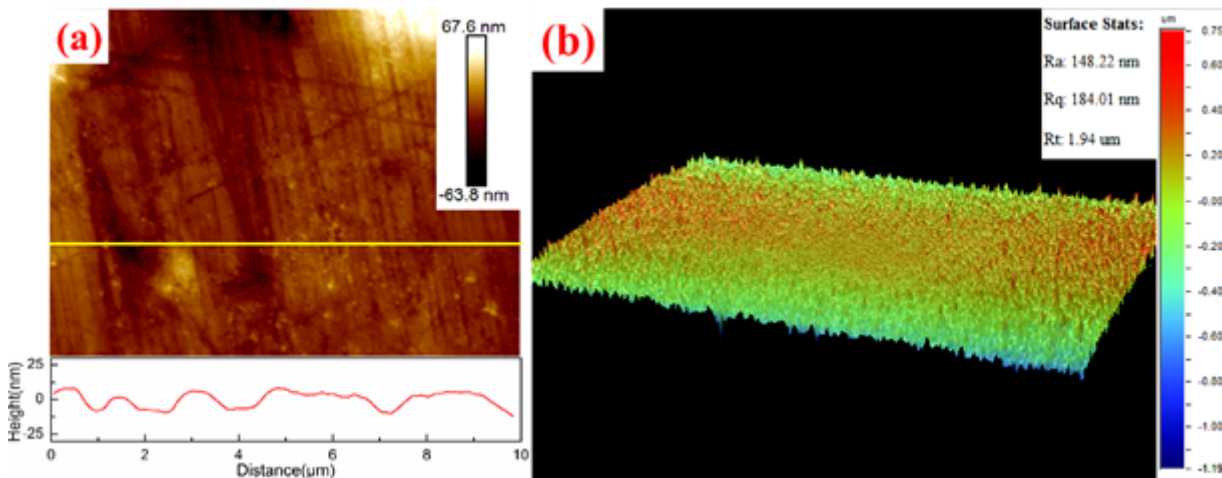
Figure 7

Surface roughness and 3D morphology before the friction test. (a): Polished teeth; (b): Mullite/ 3Y-TZP.
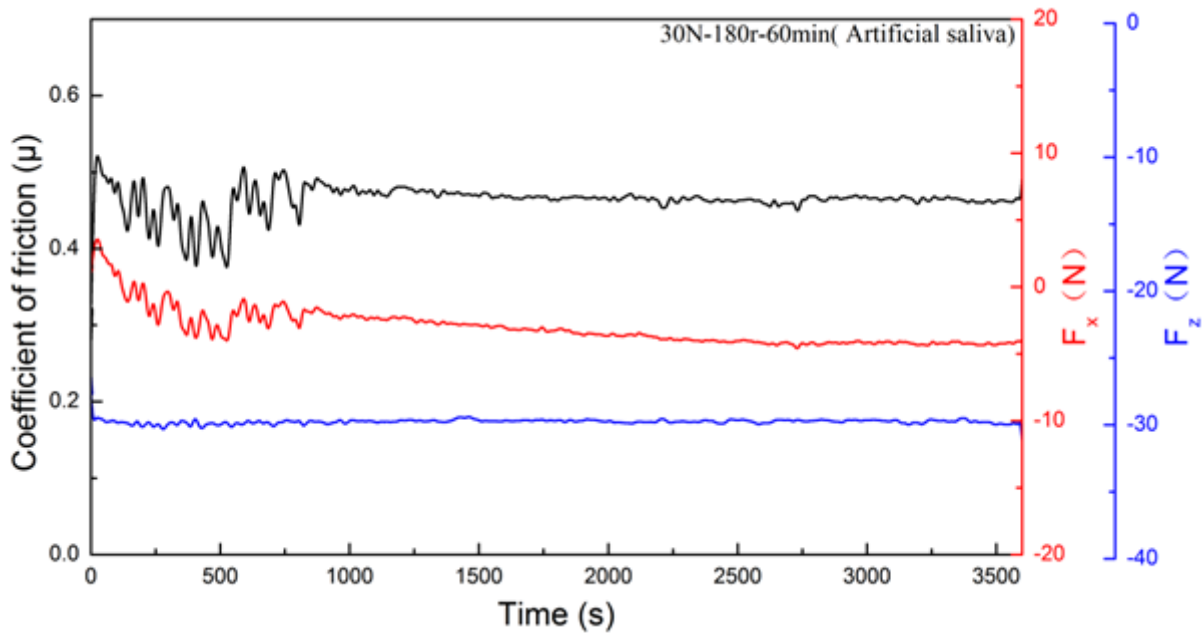
Figure 8

The curves of the coefficient of friction (μ), friction resistance (Fx) and applied load (Fz) during the friction test.
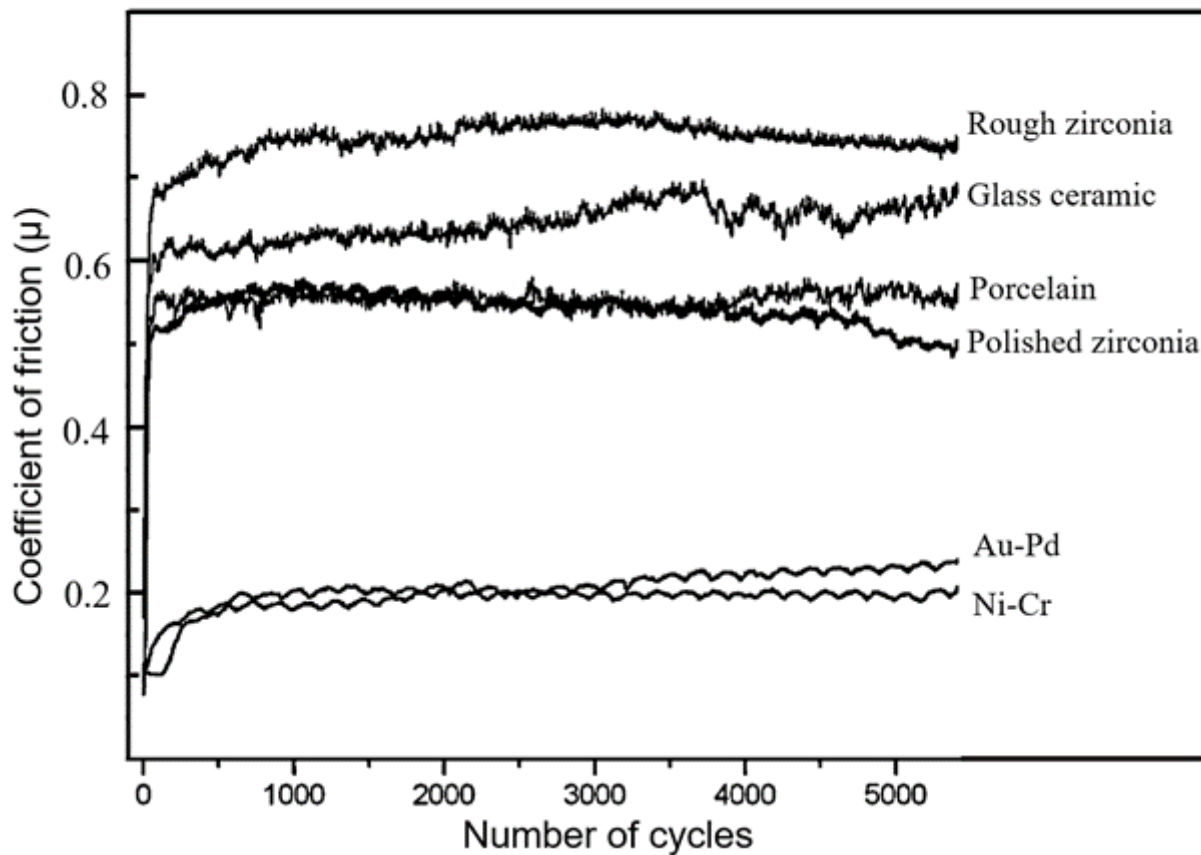
Figure 9

The coefficient of friction of natural enamel against different dental materials plotted versus the number of cycles [27].
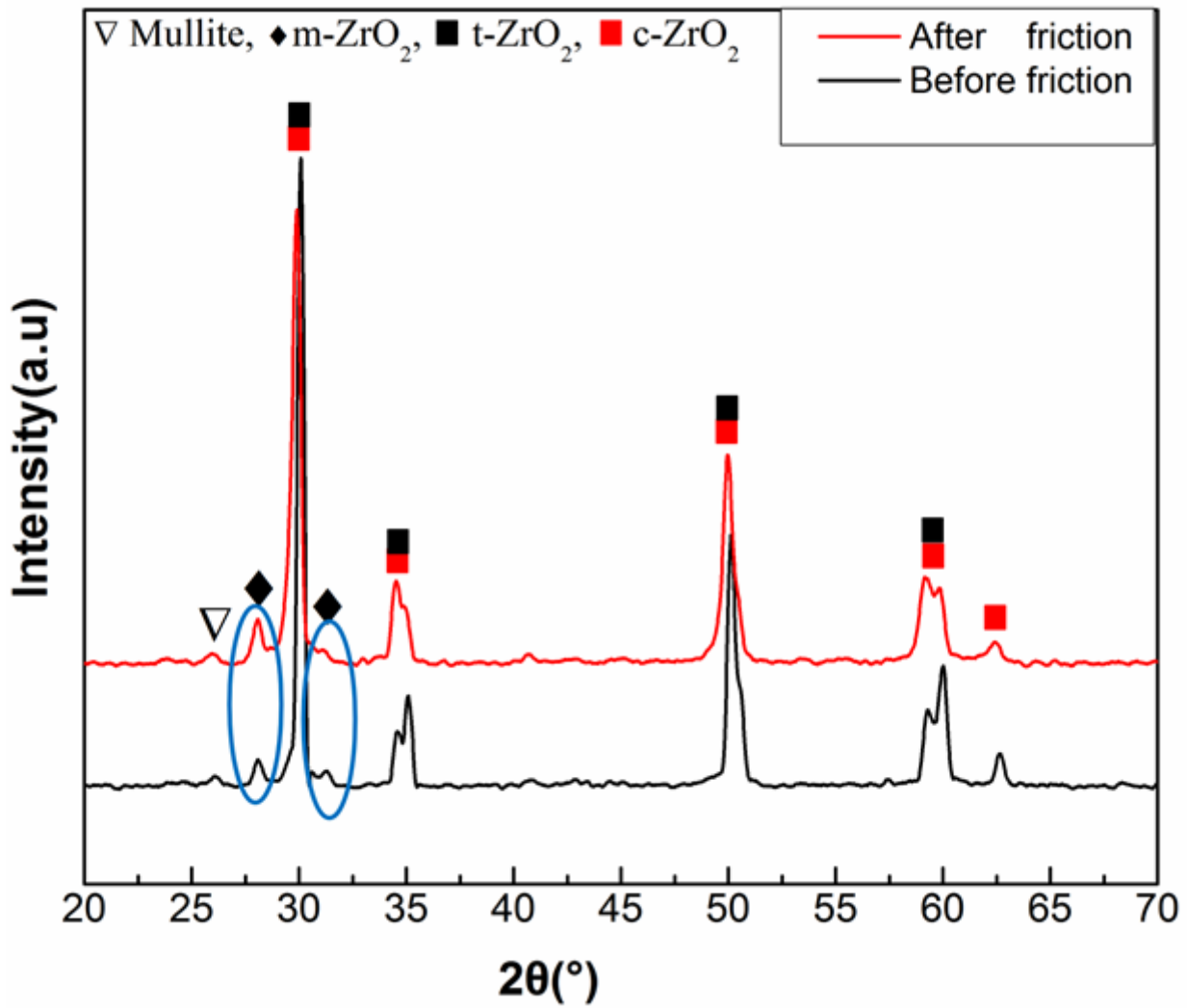
Figure 10

XRD patterns of mullite/3Y-TZP before and after the friction test.
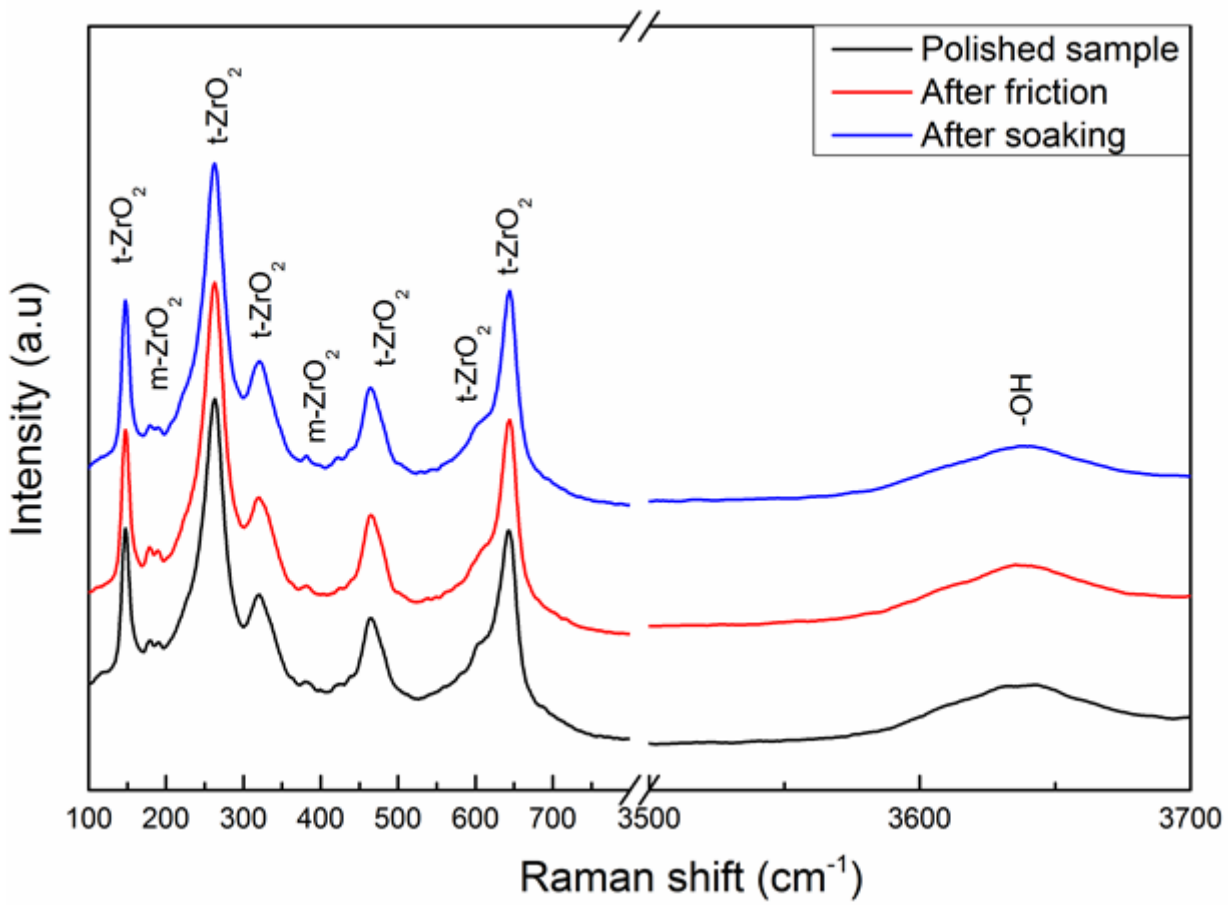
Figure 11

Raman spectrum of mullite/3Y-TZP with different methods of handling.
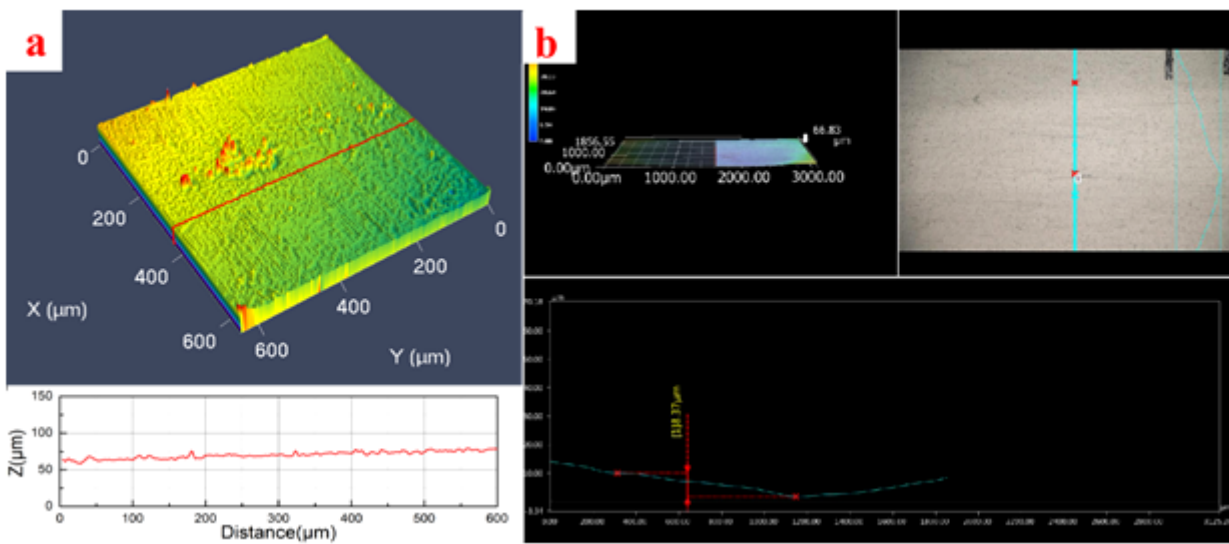
Figure 12

3D morphologies of the wear surface after friction test by different devices. (a): the enamel (LSM700); (b): Mullite/3Y-TZP (VHX-500).
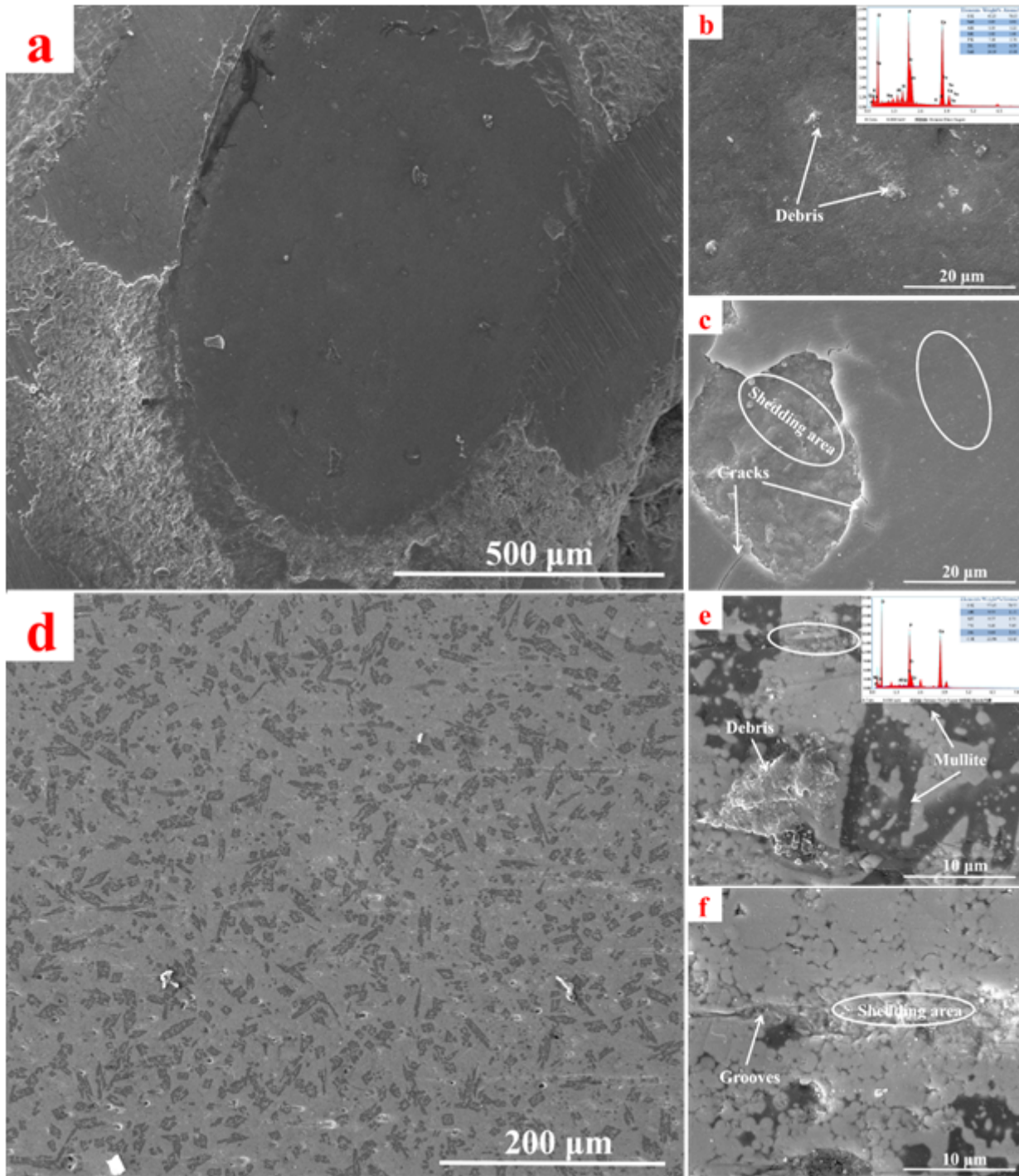
Figure 13

a): Overall microscopic morphology of the wear surface of the enamel; (b): Wear debris and its energy spectrum; (c): The local magnification of (a). (d): Overall microscopic morphology of the wear surface of mullite/3Y-TZP; (e): Wear debris and its energy spectrum; (f): The local magnification of (a).
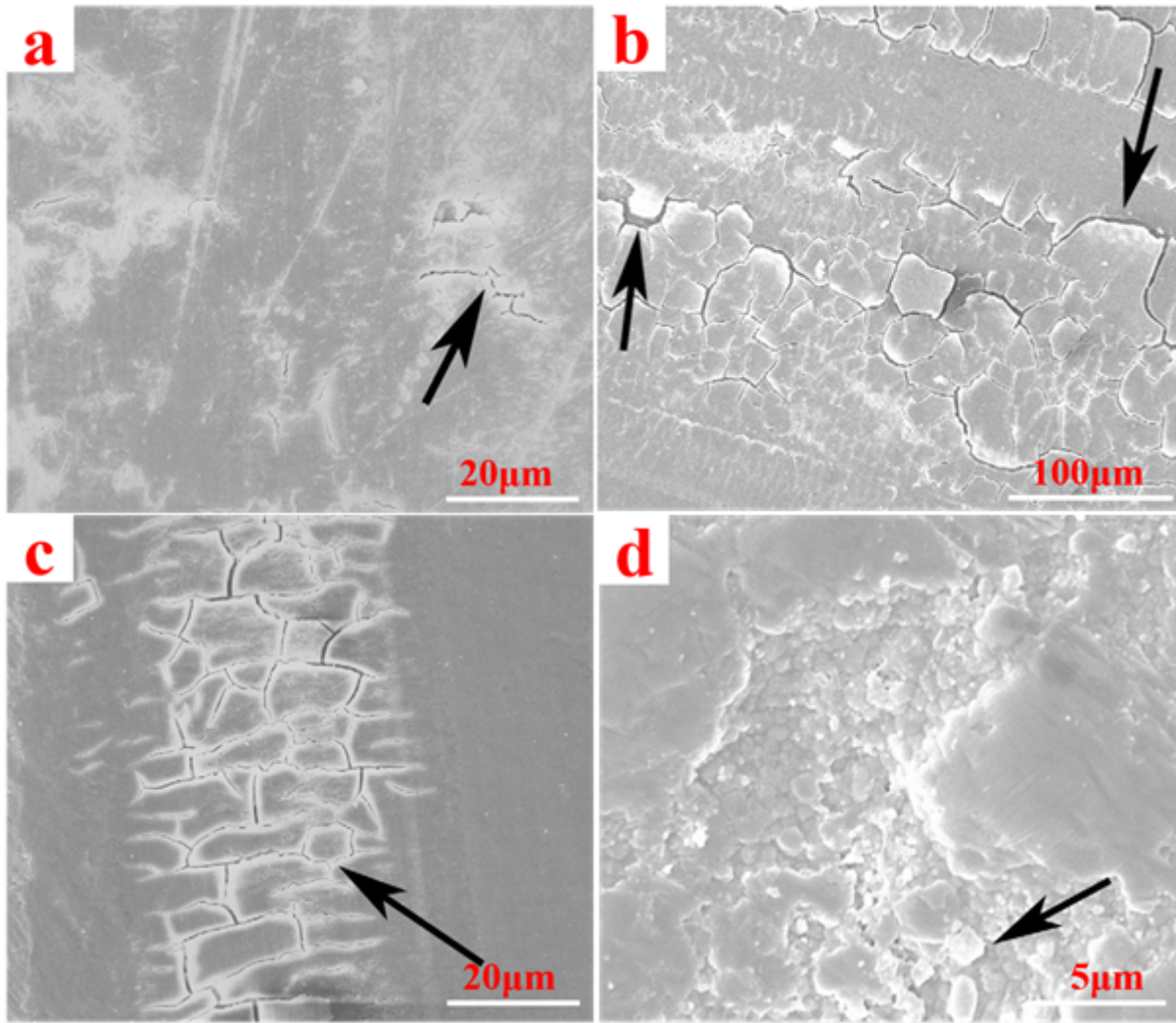
Figure 14

Micrographs showing the typical damages of enamel against polished zirconia: (a-c) the surface of enamel; (d) The surface damage of zirconia [27].
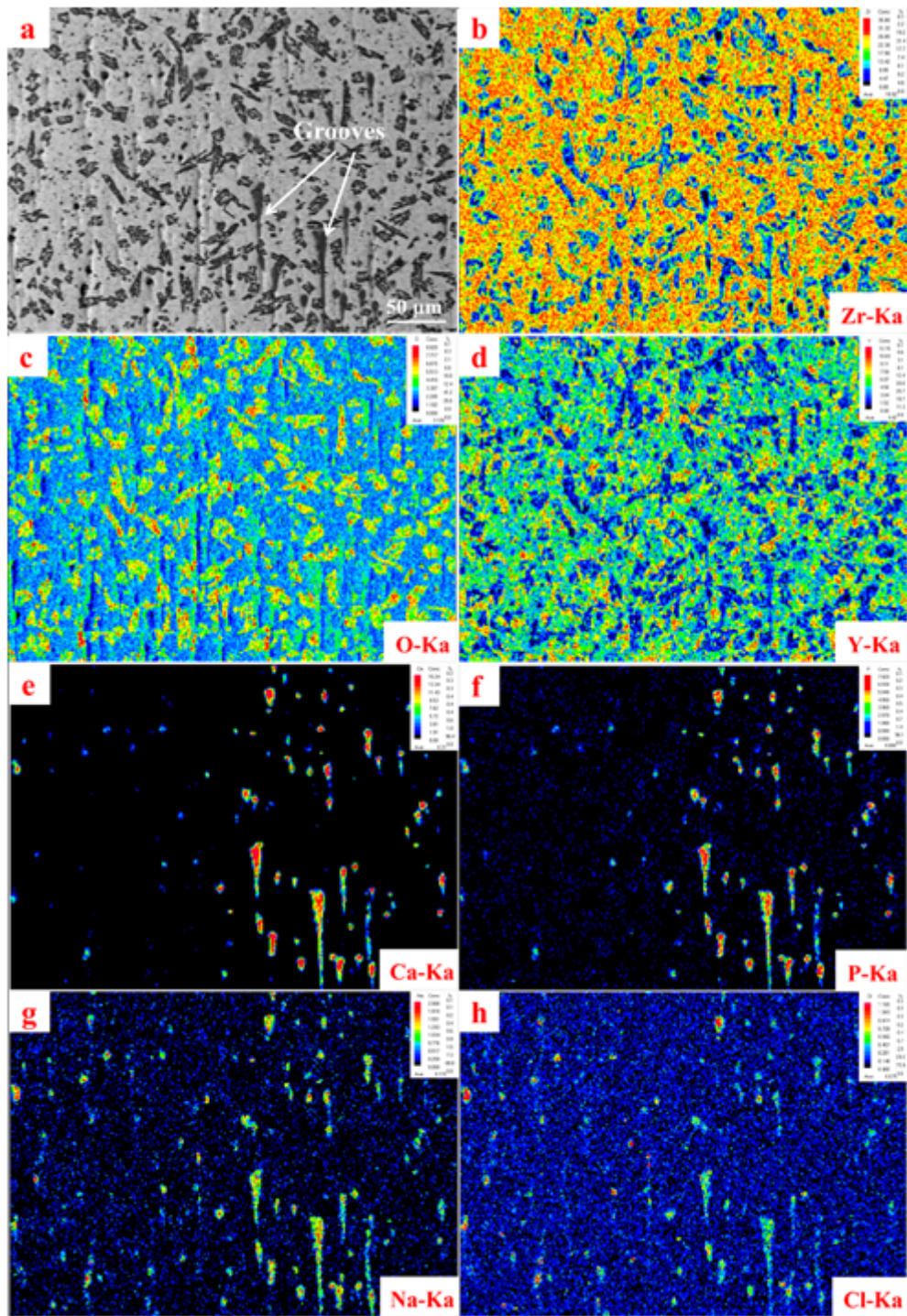
Figure 15

(a): Morphologies of the wear surface of mullite/3Y-TZP, (b-h): Distribution of various elements in this area.
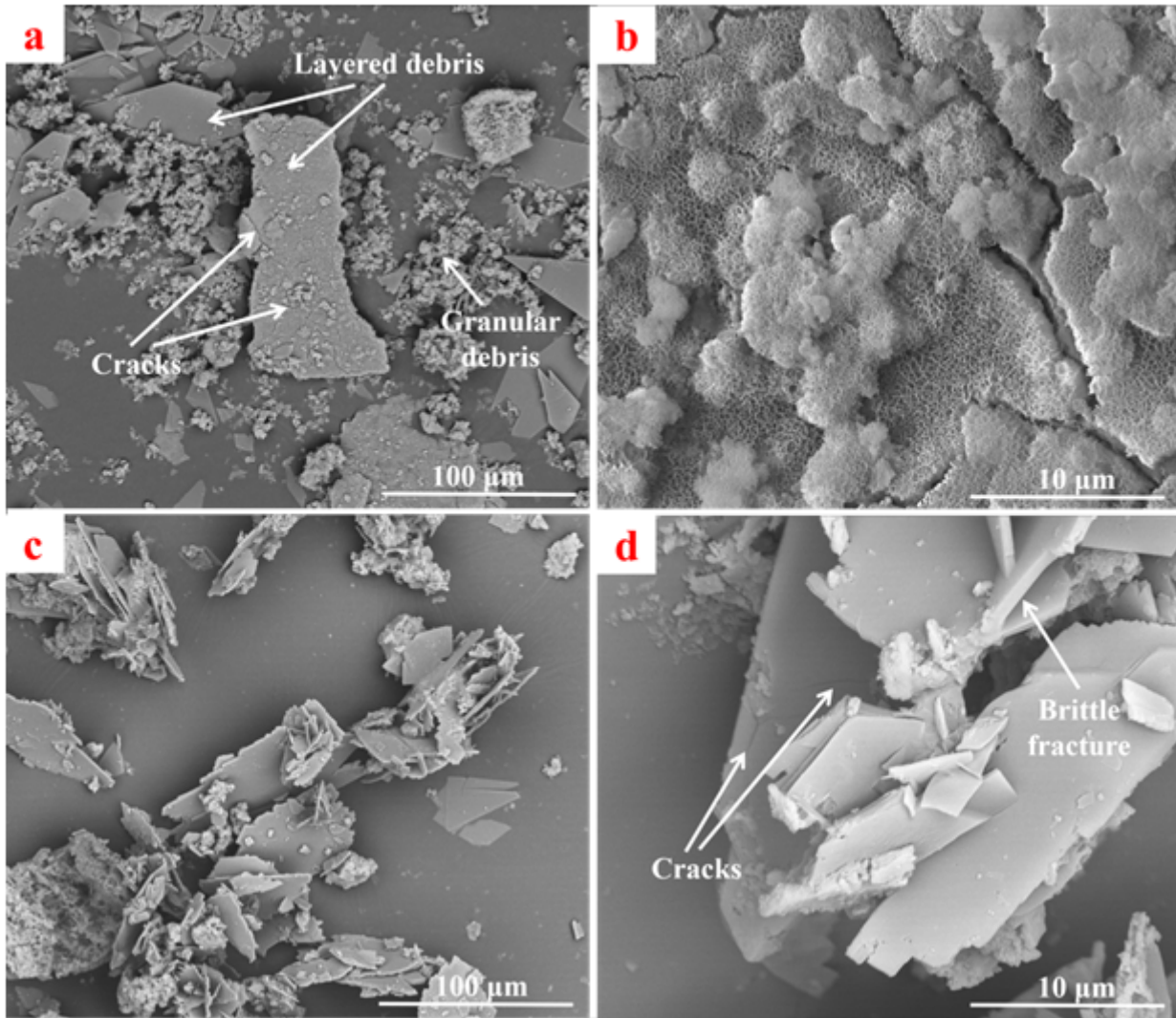
Figure 16

(a-d) Microscopic morphologies of wear debris generated during the friction test.
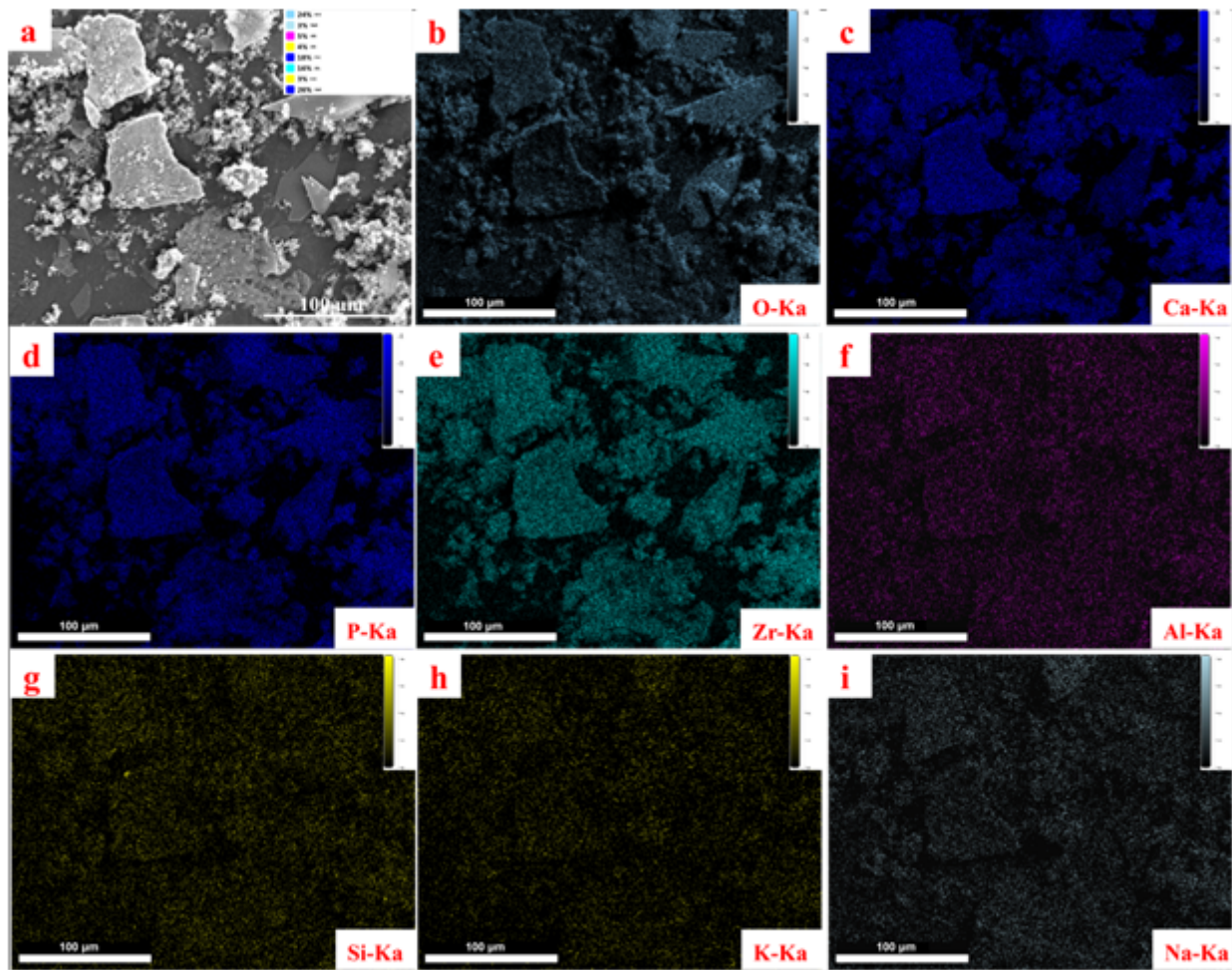
Figure 17

(a) Microscopic morphologies of wear debris; (b-i) Distribution of various elements of wear debris in this area.